Experimental studies on the resultant contact forces in drillbit-rock interaction

O.K. Ajibose *, M. Wiercigroch, A.R. Akisanya,

Centre for Applied Dynamics Research, School of Engineering, King's College,

Aberdeen University, Aberdeen, AB24 3UE, UK

Abstract

The understanding of drillbit-rock interaction is essential to the optimisation of the percussive drilling technology. It is obvious that rock fragments mainly as a result of the contact forces developed during impacts. In addition, the modelling of the dynamic response of a drilling module is possible if the contact law can be described in terms of the force and penetration. In this paper, the resultant contact force versus penetration is examined for a drillbit with conical and spherical inserts in contact with a rock. Quasi-static indentation and dynamic impact experiments are conducted on sandstone, granite and basalt. A power-law relationship is obtained between the measured resultant contact force and the penetration. The relationship is in good agreement with existing theoretical results for elastic-ideally plastic solids.

Key words: Drilling, impacts, elastic–plastic, indentation, rock

PACS:

* Corresponding author.
Email address: ajiboseok@googlemail.com (O.K. Ajibose).

1. Introduction

Percussive drilling is widely used in the mining industry for rock fragmentation. It has also found application within the oil and gas industry with increasing potential for its use in hard rock formations. The basic mechanism of rock fragmentation in percussive drilling is due to indentation loading during repeated impacts which results in the contact forces needed for the rock failure. The magnitude of the force created affects the drilling performance and is governed by the geometry of the inserts or cutters on the drillbit.

In order to optimise the percussive drilling process, it is important to understand the contact interaction between the drillbit and rock. This knowledge is essential for the development of fit for purpose drillbits and also the optimisation of the design of the drilling module. While it is worth noting that several studies [1]–[6] have been conducted to understand the rock fragmentation process and some have even proposed a bit-rock interaction model [7], only a few [8]-[10] have put forward theoretical models that relate the rock properties to the forces created at the interface. For instance, Wiercigroch *et al.* [8] have proposed a dry friction model to describe the forces at the impact interface and predict the progression achieved in an ultrasonic percussive drilling. Pavlovskaia *et al.* [9] have also used the Kelvin Voigt model to represent the contact forces in their work on drifting impact oscillator, a system similar to percussive drilling. Franca *et al.* [10] put forward a similar model for resonance hammer drilling. However, these models do not take into account the influence of the geometry of the inserts and the resulting permanent deformation or damage as a result of the high stress in the contact region.

Consequently, it is necessary to determine the actual force–penetration relationship resulting from the drillbit–rock interaction. This relationship can be incorporated into a dynamic model that captures the response of the drilling module. In the current study, experimental tests are carried out to determine the force–penetration response for indenter geometries similar to that of the drillbit inserts or cutters. We note that many drillbit inserts are conical or spherical in shape. Hence indentation tests with conical or spherical indenter will provide the necessary insight into the possible force–penetration relationship obtainable for the drillbits.

Although the drilling process is dynamic, the impact velocities are, in most cases, significantly lower than the wave speed in the rock. Hence the resulting observation for the dynamic case should not differ from the static. In this study,

static and dynamic indentation tests are carried out on some rock samples and the results are compared to verify this assumption.

The structure of this paper is as follows. First, existing theoretical approach for determining the force–penetration relationship based on contact mechanics is presented. This serves as a yardstick for the experimental results. The description of the experimental setups and procedure for quasi-static indentation of some rock samples are then outlined. Next, the observations from the experiments are presented and expressions relating the penetration to the applied load are derived based on the curve fitting of the data produced. This process is then repeated for the dynamic tests and finally the conclusions are made based on the results.

2. Indentation Contact Mechanics

Although the mechanism of rock fracture due to interaction with the drillbit inserts or cutters has been studied extensively [11,12], not much has been done to systematically establish its force–penetration relationship. However, studies in contact mechanics provide a wealth of results applicable to the present work.

It was mentioned earlier that the geometry of the cutters or inserts on drillbits is close to conical or spherical. Thus we assume the drillbit–rock interaction is analogous to the case of a rock loaded by multiple conical or spherical indenters.

Love [13] showed that the indentation force versus penetration response for a medium at an impact velocity that is much lower than the wave speed did not differ from that obtained when it was quasi–statically loaded. Furthermore, it was established that when the region of contact was very small compared to the overall dimensions of the contact bodies then the influence of reflected waves on the contact zone was insignificant such that the deformed region could be regarded as being under a quasi-static loading [14]. These arguments apply to the drillbit–rock interaction problem in percussive drilling. Thus the results from previous studies on quasi-static indentation theory and experiments are relevant to the current study.

Foremost amongst such results are those by Johnson [15] , who showed that the mean contact pressure between a rigid conical indenter and an elastic–ideally plastic half space is given by

$$\frac{p_m}{Y} = \frac{2}{3}\left(1 + \ln\left[\frac{E\tan\beta}{6Y(1-\nu)} + \frac{2(1-2\nu)}{3(1-\nu)}\right]\right), \tag{1}$$

where E is the elastic modulus of the medium, Y is its yield strength, ν is the Poisson's ratio and β is the angle between the conical surface and the elastic-plastic half space (see Fig.1(a)). The results of experiments carried out on metals [16,17] are in reasonable agreement with (1). By considering static equilibrium of forces, the indentation force

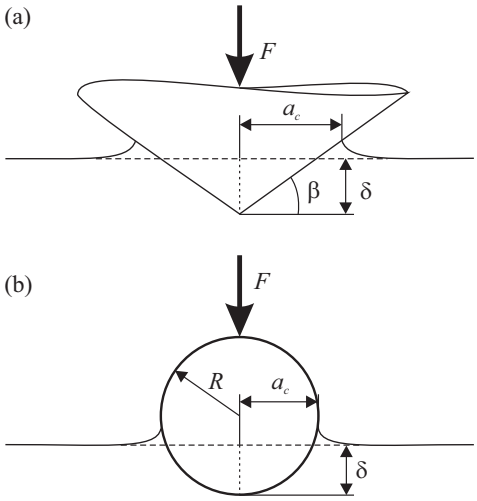

Figure 1. Penetration of a medium by (a) conical and (b) spherical impactors (pile–up exaggerated). Adapted from [15].

during the loading phase, F , and penetration, δ, can be shown to be of the form

$$F = \frac{2}{3}\frac{Y\pi\delta^2}{\tan^2\beta}\left(1 + \ln\left[\frac{E\tan\beta}{6Y(1-\nu)} + \frac{2(1-2\nu)}{3(1-\nu)}\right]\right). \tag{2}$$

Hence the force–penetration relationship can be written in the form

$$F = K_c\delta^2, \tag{3}$$

where K_c is given as

$$K_c = \frac{2}{3}\frac{Y\pi}{\tan^2\beta}\left(1 + \ln\left[\frac{E\tan\beta}{6Y(1-\nu)} + \frac{2(1-2\nu)}{3(1-\nu)}\right]\right). \tag{4}$$

Here and thereafter subscript c is used to denote parameters associated with conical indenters.

Similarly, Stronge [18] showed that the indentation force versus penetration relationship for a rigid spherical indenter on an elastic–ideally plastic material (Fig.1(b)) is of the form

$$\frac{F}{F_y} = \begin{cases} \left(\dfrac{\delta}{\delta_y}\right)^{\frac{3}{2}} & \text{if } \dfrac{\delta}{\delta_y} \leq 1, \quad \text{elastic regime,} \\ \left(\dfrac{2\delta}{\delta_y} - 1\right)\left[1 + 3.3^{-1}\ln\left(\dfrac{2\delta}{\delta_y} - 1\right)\right] & \text{if } 1 < \dfrac{\delta}{\delta_y} \leq 84, \quad \text{elasto-plastic regime,} \\ 2.55\left(\dfrac{2\delta}{\delta_y} - 1\right) & \text{if } \dfrac{\delta}{\delta_y} > 84, \quad \text{fully plastic regime,} \end{cases} \tag{5}$$

where F_y and δ_y are the force and penetration values, respectively, at the onset of plastic yield. The load at yield F_y and the corresponding penetration δ_y for a rigid spherical indenter of radius R are given by [19]

$$\begin{aligned} F_y &= 23.25\left(\frac{R^2Y^3}{E^2}\right) \\ \delta_y &= 6.75R\left(\frac{Y}{E}\right)^2 \end{aligned} \tag{6}$$

where R is the radius of the spherical indenter, and Y and E_s are the uniaxial yield strength and elastic modulus of the elastic-ideally plastic half space.

Similarity analysis and experimental studies in [21] suggest that the force–penetration relationship during a quasi-static indentation of an elastic-ideally plastic solid by a rigid spherical indenter is of the form

$$F = K_s\delta^{n_s}, \tag{7}$$

where K_s and n_s are material and geometric constants and subscript s is used to identify parameters associated with spherical indenters. The force–penetration response (5) proposed by Stronge [18] can be described by the power law relation (7).

These power–law force–penetration relations, which were originally developed for rigid indenters on elastic-ideally plastic materials, compare reasonably well with the results obtained for some rocks like sandstone [20,22] and some ceramics [23]. The validity of the relations (3) and (7) for static and dynamic indentation of sandstone, granite and

basalt is experimentally examined in the current paper.

3. Quasi–Static Indentation Tests

Percussive drilling generally involves low velocity impacts of a relatively smaller drilling module with a significantly larger earth-crust. The results of the quasi–static indentation of rocks presented in this paper are therefore applicable to this method of rock removal. In the following, the design of the indenters and the experimental setup used to establish the force–penetration relationship via quasi-static loading and the design of the indenters are described.

3.1. *Design and manufacture of indenters*

The drillbit inserts or cutters are considered as conical or spherical indenters. In order to ensure that results are not distorted due to poor indenter design, certain factors have been considered.

A steel conical indenter was designed with the base angle of the cone equal to 22.5° (see Fig. 2 (a)) to ensure the indentation angle was similar to that used in Vickers hardness tests. In addition, the tip of the cone was rounded to a radius of 1 mm while the base diameter of the cone was 10 mm for ease of manufacture. On the other hand, the spherical indenter was made by fitting a 10 mm diameter spherical steel ball into a hollow cylinder of the same inner diameter and 12 mm outer diameter (see Fig. 2 (b)). The conical indenter and the hollow cylinder were made from mild steel. The assembly was then screwed onto a connector.

After machining, the indenter and the cylinder were case-hardened by heating to 900°C, and subsequently dipping into Kasenite powder until they cooled. This process was repeated once more to force the hardening deeper. The pieces were then reheated to the same temperature of 900°C and quenched in water. They were subsequently polished to remove the extra powder on their surfaces. Vickers hardness test was carried out on a piece of mild steel that has undergone the same heat treatment. This gave a hardness value of $H_V = 635$ which is greater than that for sandstone ($H_V = 38$), granite ($H_V = 315$) and basalt ($H_V = 400$).

(a) (b)

Figure 2. A schematic of the (a) conical and (b) spherical indenter. The conical indenter base angle was 22.5°, while the diameter of the sphere was 10 mm.

3.2. *Experimental set–up and Procedure*

Quasi–static indentation tests were carried out on samples of sandstone, granite and basalt. The samples were in the form rectangular blocks with dimensions $50\ \mathrm{mm} \times 50\ \mathrm{mm} \times 25\ \mathrm{mm}$. The indenter was connected to a load cell on a screw–driven testing machine via a threaded connector (see Fig.3). The rock was loaded in displacement control at crosshead speeds of 0.1, 1, and 5 mm/min for sandstone. In the case of the basalt and granite , which are harder rocks, the tests were carried out at crosshead speeds of 1 and 2 mm/min. The load was applied until it reached between 7.5 kN and 12 kN, after which the sample was completely unloaded by reversing the motion of the crosshead. The displacement of the crosshead, which was measured by an LVDT, and the load were continuously recorded during the loading and unloading phases using a computerised data logger. We note that the overall dimensions of the samples and the contact area with the indenter causes the stiffness of the samples to be much smaller than the stiffness of the testing machine. Hence, the displacement captured by the LVDT is not influenced significantly by the stiffness of the testing machine.

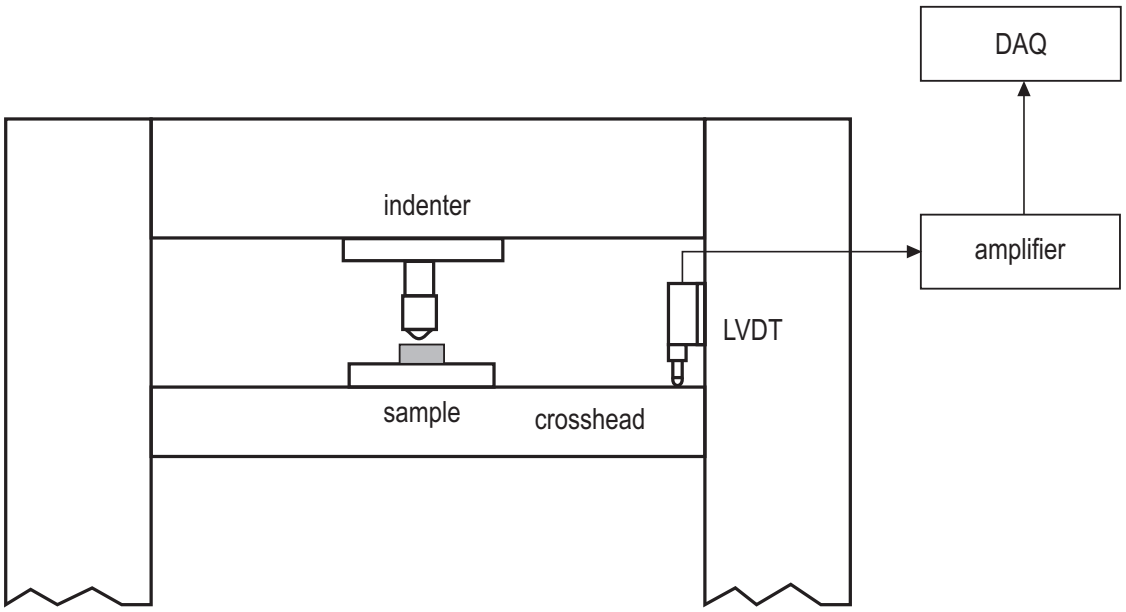

Figure 3. A schematic of the set-up for static tests on the INSTRON 1185 material testing machine.

3.3. *Observations and deductions*

The results of the quasi-static indentation experiments on the rocks provide insight into the contact interactions between the bodies. It was observed that the indentation produced imprints on the rocks. Some specimens were loaded until fracture. Figure 4 shows a sandstone specimen that was subject to indentation loading using a spherical indenter and subsequently cut to reveal the damaged zone. A sandstone specimen loaded to failure using a conical indenter is shown in Fig. 5. In both cases, a localised damage zone was formed directly below the imprint while the rest of the material was undamaged. The non-linear load versus displacement response and the residual surface impression are indication of a "quasi-plastic" deformation [23].

In order to obtain the contact law from the experiments the load readings were plotted against the displacement data obtained for each test. A typical example is shown in Fig. 6 for a conical indenter on sandstone. The loading and unloading phases are also plotted separately in Fig. 7 (a) and (b). The load–displacement response for granite and basalt is qualitatively similar to that for sandstone but with lesser final penetration as a result of the greater hardness of these rocks.

These figures reveal that a non–linear relationship exits between the force and the penetration for both the loading and the unloading phases of the indentation. This is observed for all test speeds used, as such the response does not

Figure 4. The damaged zone formed by spherical indenter on sandstone .

Figure 5. The damaged zone formed by conical indenter on sandstone.

qualitatively depend on the rate of loading. The load–penetration curves shown in Fig. 6 suggest that the indentation behaviour of the rock samples is similar to that of metals as observed by Kicks [25], Meyer [26] and Attaf [27]. Hence, the crushed zone below the indenter is in a “quasi-plastic” state as suggested by Lawn [23] for ceramics since the force–penetration response is similar to that of an elastic-plastic medium.

The load–displacement curves can be fitted to a power–law type force–displacement relationship of the form

$$F = K\delta^n, \tag{8}$$

where δ is the displacement of the indenter into the rock in the loading phase or the relative displacement with respect to the deformation of the rock at the end of the unloading phase. F is the force, K is a material constant and n is an exponent whose value depends on phase of the loading, i.e. loading or unloading phase.

If the values of n and K are determined, then it is possible to develop a dynamic model using this contact force law to represent the resistance of the rock to the motion of the drilling module and hence determine its response and optimise its design.

In order to fit the experimental data to the proposed function, the linear least square method [25] is used to determine possible values of n and K. The following paragraphs outline the process.

Equation (8) is linearised by setting $x = \delta^n$ to obtain

$$F = Kx, \tag{9}$$

The values of n and the corresponding values of K that give the best approximation to the measured data are determined using the linear least square method. To achieve this, first it can be shown that for a given value n_i, ($i = 1, 2, 3...q$), where q is the total number of possible exponents being considered, the corresponding K_i is obtained from the expression

$$K_i = \frac{\sum x_j F_j}{\sum x_j^2} \tag{10}$$

where $j = 1, 2, .., k$ and k is the number of data points on the loading or unloading curve. This provides the value of K_i for each assumed value of n_i. The best (n_i, K_i) combination is that which gives the minimum deviation from the measured response. For each n_i and the corresponding K_i, the predicted force, $K_i\delta_j^{n_i}$, is compared with the measured force F_j at a displacement δ_j. The square of the deviation, ζ_j, between the measured and the predicted force at each of the measured data point (δ_j, F_j) is defined as

$$\zeta_j = (F_j - K_i x_j)^2 \tag{11}$$

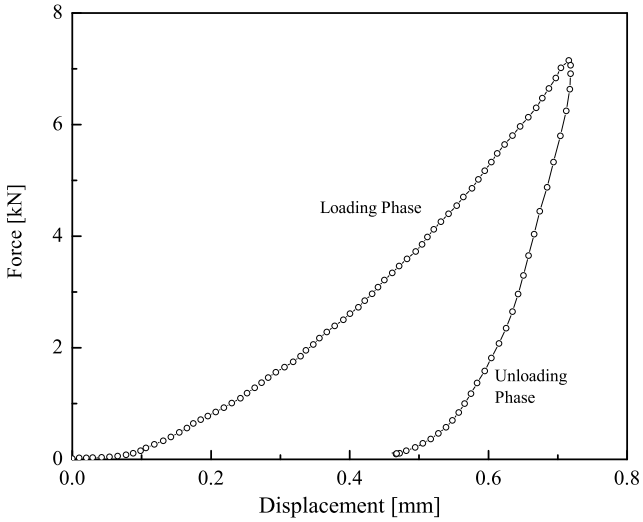

Figure 6. Force–displacement response for the loading and unloading phases of conical indentation at 0.1 mm/min loading

(a)

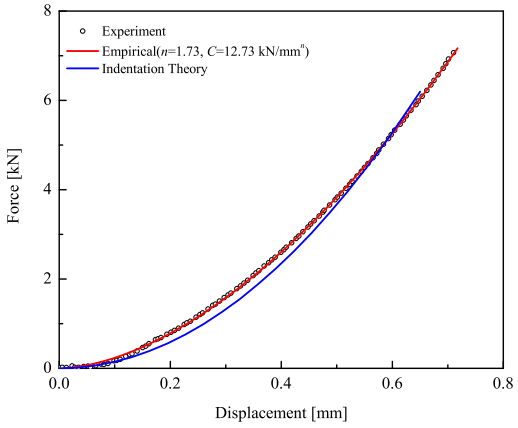

(b)

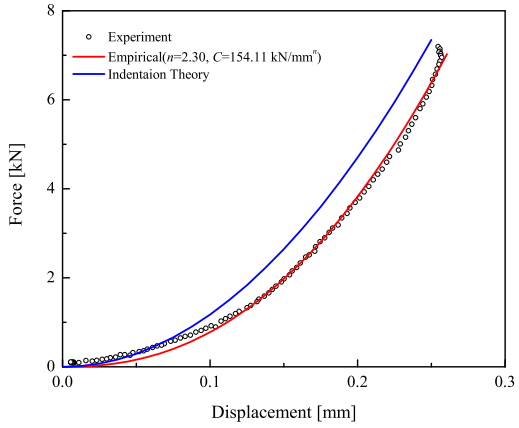

Figure 7. Comparison between the measured and empirical relation of the force–displacement response for a conical indenter on sandstone (a) loading and (b) unloading(Displacement in (b) is relative to deformation at the end of the unloading phase).

The maximum value D_i of the deviation associated with a given combination of material constants (n_i, K_i) for a given measured data set is given by

$$D_i = \max\left[\zeta_j\right] \tag{12}$$

Figure 8 shows the effect of the assumed exponent $n = n_i$ on the maximum deviation D_i. The best value of n is that which minimises the maximum deviation. It is noted that for the conical indenter loading at $0.1\mathrm{mm/min}$, the best value of $n = n_i = 1.73$ with a corresponding value of $K = K_i = 12.73$ kN/mm$^{1.73}$.

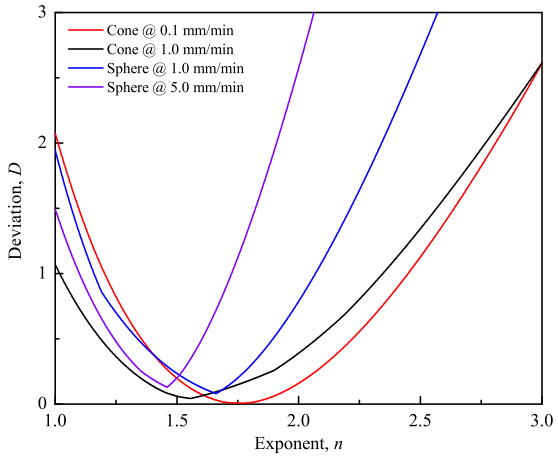

Figure 8. Graphical representation of method of estimation of best n for static loading at various test speeds for the conical and spherical indenters (D in kN^2)

Tables 1 and 2 give a list of the values of n and K estimated for the conical and spherical indenters respectively in the loading and unloading phase at different test speeds. We note that the value of n in the loading phase is smaller than that for the unloading phase. The material constant n is relatively independent of the loading speed for the range of speeds considered. However, both K and n depend on the material and indenter geometry. The discrepancies in the value of n and K for identical test conditions can be attributed to the heterogeneity of the rock samples. A summary of the average values of K and n are presented in Table 3.

Figure 7 shows a comparison between the theoretical results (eqn.(3)), the experimentally measured response and the empirical curves based on eqn (7) and average values of K and n in Table 3. It is observed that all three curves are

Table 1
Values of the exponent n and constant K for a conical indenter during the loading and unloading phases of the static tests.

Indenter	Rock type	Test Speed	Loading Phase		Unloading Phase	
		[mm/min]	K $[\mathrm{kN/mm}^n]$	n	K $[\mathrm{kN/mm}^n]$	n
Cone	Sandstone	0.1	12.72	1.73	154.11	2.30
Cone	Sandstone	1.0	13.25	1.53	131.25	1.92
Cone	Sandstone	5.0	12.88	1.48	173.36	2.35
Cone	Basalt	1.0	118.47	2.10	205.90	1.94
Cone	Basalt	1.0	116.33	1.68	208.96	1.95
Cone	Basalt	1.0	130.00	1.98	195.46	1.88
Cone	Basalt	1.0	124.36	1.78	152.49	1.65
Cone	Basalt	2.0	87.42	1.38	176.71	1.69
Cone	Basalt	2.0	119.86	1.74	169.86	1.76
Cone	Basalt	2.0	115.56	1.70	158.26	1.69
Cone	Basalt	2.0	157.71	1.91	150.31	1.64
Cone	Basalt	2.0	107.08	1.53	172.75	1.75
Cone	Granite	1.0	87.67	1.65	117.91	1.74
Cone	Granite	1.0	68.11	1.40	132.56	1.77
Cone	Granite	1.0	83.65	1.59	124.94	1.77
Cone	Granite	1.0	83.64	1.51	140.15	1.73
Cone	Granite	2.0	91.11	1.56	115.00	1.61
Cone	Granite	2.0	83.46	1.45	125.68	1.69
Cone	Granite	2.0	103.39	1.58	136.93	1.74
Cone	Granite	2.0	75.63	1.38	119.24	1.67
Cone	Granite	2.0	99.76	1.65	126.59	1.70

reasonably close. Therefore, we conclude that the results obtained in equations (3) and (7) can be used for the analysis of the quasi-static indentation of the rocks considered in this study.

4. Dynamic Tests

On the basis of the earlier arguments that the rock fragmentation process associated with impacts at velocities lower than the elastic wave speed of the medium by an indenter is identical to that due to quasi–static loading, the outcomes

Table 2
A summary of the exponent n and constant K values for a spherical indenter during the loading and unloading phases of the static tests.

Indenter	Rock type	Test Speed	Loading Phase		Unloading Phase	
		[mm/min]	K $[\mathrm{kN/mm}^n]$	n	K $[\mathrm{kN/mm}^n]$	n
Sphere	Sandstone	0.1	20.88	1.33	153.57	2.02
Sphere	Sandstone	1.0	23.90	1.67	147.03	2.14
Sphere	Sandstone	5.0	21.59	1.47	175.52	2.75
Sphere	Basalt	1.0	61.02	1.35	132.99	1.89
Sphere	Basalt	1.0	65.24	1.43	150.99	1.99
Sphere	Basalt	1.0	106.31	1.85	293.03	2.56
Sphere	Basalt	1.0	69.27	1.37	142.13	1.81
Sphere	Basalt	1.0	82.19	1.52	234.78	2.18
Sphere	Basalt	2.0	66.26	1.33	152.52	1.85
Sphere	Basalt	2.0	72.81	1.42	148.26	1.88
Sphere	Basalt	2.0	67.72	1.34	147.60	1.82
Sphere	Basalt	2.0	71.34	1.38	176.37	1.95
Sphere	Basalt	2.0	72.70	1.45	142.57	1.91
Sphere	Granite	1.0	67.66	1.45	99.97	1.72
Sphere	Granite	1.0	67.46	1.45	89.20	1.65
Sphere	Granite	1.0	64.91	1.39	101.63	1.74
Sphere	Granite	1.0	67.51	1.46	117.24	1.85
Sphere	Granite	2.0	71.45	1.47	104.47	1.75
Sphere	Granite	2.0	68.75	1.48	118.34	1.87
Sphere	Granite	2.0	73.05	1.54	119.04	1.88
Sphere	Granite	2.0	65.53	1.37	115.86	1.78

of the quasi-static experiments presented above were considered to be valid for the dynamic process. However, it is important to confirm that the force–penetration characteristics of the indentation process still remain the same for this kind of impact. To achieve this, an impact–fracture rig was designed to simulate the fragmentation of rocks at low collision speeds, and also to determine the resulting contact force–displacement relationship for rocks which would be applicable in a dynamic model for percussive drilling.

Table 3
A summary of the average values of the exponent n and constant K values for conical and spherical indenters during the loading and unloading phases of the static tests.

Indenter	Rock Type	Loading Phase		Unloading Phase	
		K $[\mathrm{kN/mm}^n]$	n	K $[\mathrm{kN/mm}^n]$	n
Cone	Sandstone	12.95 ± 0.27	1.58 ± 0.13	152.90 ± 21.09	2.19 ± 0.24
Cone	Basalt	119.64 ± 18.72	1.76 ± 0.22	176.74 ± 22.16	1.77 ± 0.12
Cone	Granite	86.27 ± 10.99	1.53 ± 0.10	126.56 ± 8.61	1.71 ± 0.05
Spherical	Sandstone	22.12 ± 1.58	1.49 ± 0.17	158.71 ± 14.92	2.30 ± 0.39
Spherical	Basalt	73.49 ± 12.85	1.44 ± 0.15	172.12 ± 51.50	1.98 ± 0.22
Spherical	Granite	68.29 ± 2.77	1.45 ± 0.05	108.22 ± 10.99	1.78 ± 0.08

4.1. *Experimental set–up for dynamic indentation*

The design of the impact fracture rig is based on the slider–crank mechanism shown in Fig. 9. The flywheel is driven by an adjustable speed DC motor via a belt drive. The belts are mounted on equal diameter wheels to ensure that the flywheel spins at the same angular frequency as the electric motor. The flywheel is then linked via the connecting rod to the slider which is constrained to move within the guides resulting in an oscillatory motion in the horizontal direction. The guide surfaces were lubricated to minimise the effect of friction.

Accurate measurement of contact force is crucial to the success of the experiment. This is achieved by incorporating force measurement ability to the design of the slider. The slider was made up of three pieces. The first is a solid cylinder block made from aluminium to which the connecting rod is attached. The second part is a hollow cylinder, on which strain gauges are mounted thereby acting as a load cell. This is attached at one end to the free side of the aluminium cylinder, and at the other end to the third piece made in the form of a frustum which screws onto it. A conical indenter (base angle = 60°) is mounted on the frustum and a flat plate is also attached to it. The indenter on the slider penetrates the rock sample which is mounted on a fixed rig, with the rock face perpendicular to the axis of motion of the slider as shown in Fig. 9. A LVDT is attached to the flat plate on the slider to record the displacement of the slider as it comes in contact with the rock.

To ensure impact occurs, the fixed rig for the rock is positioned within the stroke of the slider. Also, it is noted that the connecting rod slides within a slot in the flywheel. This guarantees a motion of the flywheel which continues

freely during the impact of the slider with rock and prevents any jerky motion.

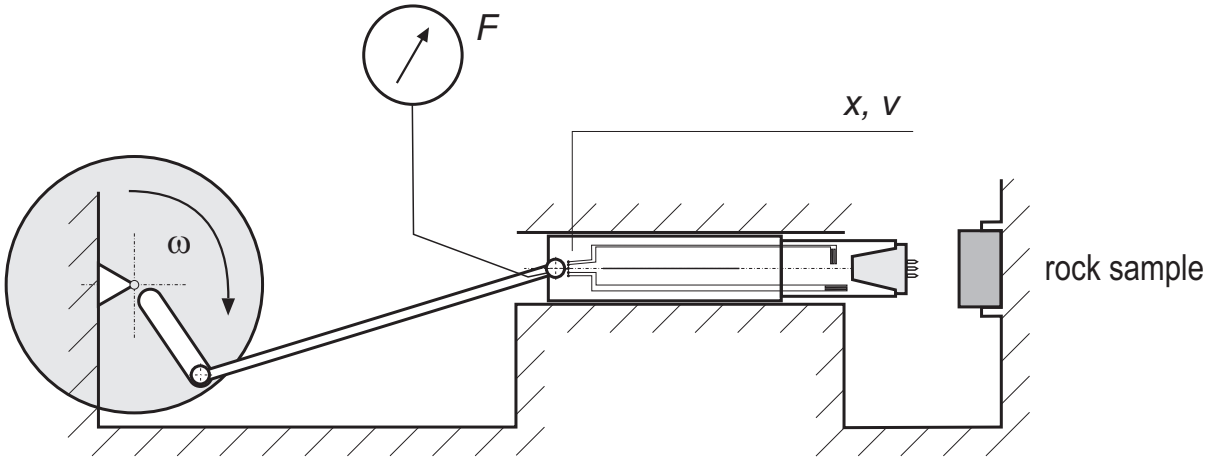

Figure 9. A schematic of the experimental rig for the dynamic tests showing the different components.

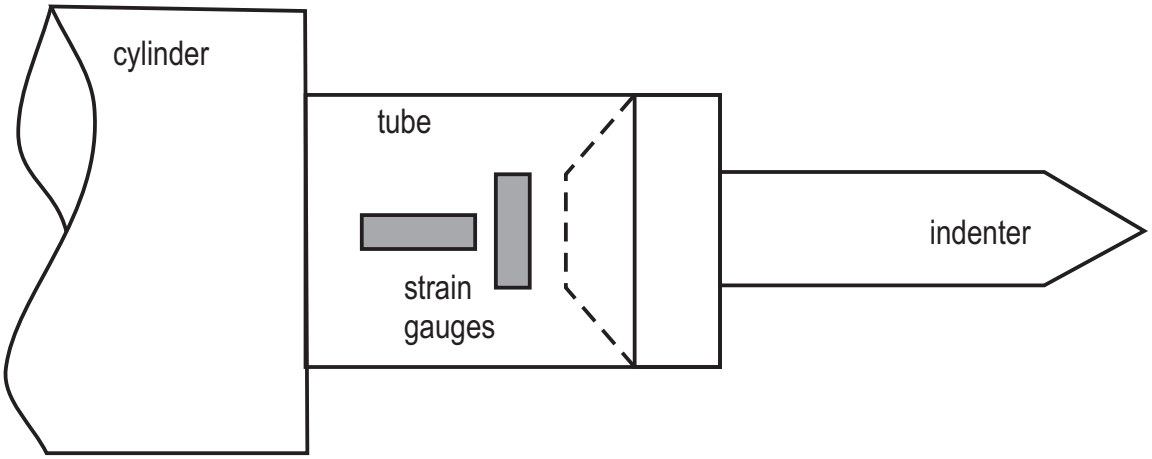

Figure 10. A schematic of the load cell assembly for the dynamic test rig.

4.2. *Measurement of force and displacement*

As mentioned earlier, the success of the experiment is pivoted on accurate measurement of the force and displacement during impact. This subsection describes the design of the load cell and the set-up for the LVDT in detail.

The load cell was made by placing strain gauges on the hollow cylinder that formed part of the slider. The indenter

was mounted on a frustum which was screwed onto the cylinder as shown in Fig. 10. The hollow cylinder was made from AISI 1050 stainless steel with an outer diameter of 32 mm and inner diameter of 28 mm, while the length was 45 mm. Four strain gauges (FLU-5-11, Gauge Factor$= 2.12$, Resistance$= 120\ \Omega$) were mounted on the hollow cylinder and connected to make up a full Wheatstone bridge, with two gauges in the axial direction on opposite sides of the cylinder and two along the circumference, again, on two opposite sides. This configuration ensures that only tensile and compressive forces are captured by the setup and no torque or bending load influenced the change in the output voltage of the bridge. The compressive force measured by this setup is given by [29]

$$P = 2A\frac{\Delta e}{S_g V}\frac{E_c}{1+\nu}, \tag{13}$$

where A is the cross-sectional area of the hollow cylinder, Δe is the output voltage of the bridge, $S_g = 2.12$ is the gauge factor, V is the excitation voltage, E_c is the elastic modulus of the cylinder and ν is the Poisson's ratio of the hollow cylinder. The load cell was calibrated by uniaxial compression on a screw–driven test machine.

The displacement of the indenter into the rock was measured using a non–contacting LVDT (Macro sensor: PSR-4500-006) which was connected to the slider via a flat plate (see Fig.9). The LVDT is classified as an instrument with a dead time delay i.e. the result obtained from it lags behind the actual occurrence of the event [31]. This time delay becomes more pronounced in dynamic loading. To overcome this, the peak displacement measured for each impact was assumed to coincide with the peak force obtained from the load cell. Therefore, data points corresponding to the peak displacement were moved back in time to match the data point corresponding to the peak load. The start of the loading phase was subsequently estimated by assuming it lags behind that obtained from the load cell by the same magnitude as for the peak displacement.

4.3. *Procedure for dynamic tests*

First, the slider was positioned to allow it to acquire reasonable impact velocity when it moved. The rock piece was then fitted into its holder and tightened to ensure it was locked in place. The DC motor frequency was set to the desired values. The motor was then switched on and the load and displacement readings taken from the load cell

and LVDT respectively. After few impacts, the motor was switched off and the frequency changed. The rock was then positioned such that a new surface was available for impacts and the test was then be repeated. In this study, the impact frequencies used were 3Hz, 4Hz and 5Hz.

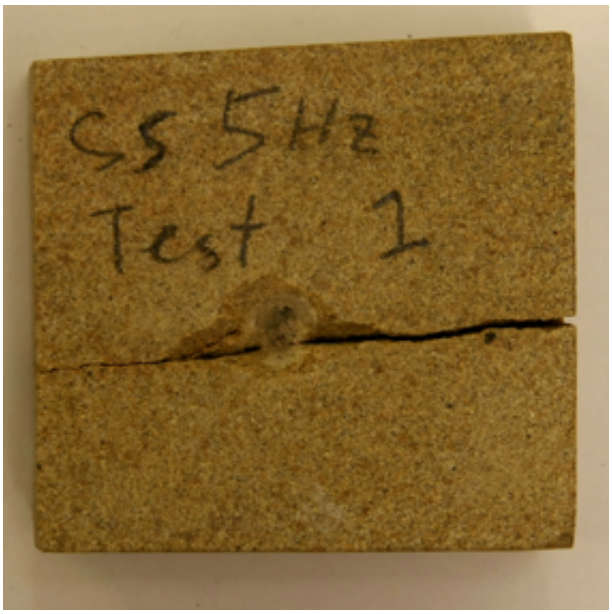

(a)

(b)

Figure 11. Formation of damaged zone in dynamic loading of sandstone. Damage as seen through (a) top view and (b) cut section.

4.4. *Observations and deductions from dynamic tests*

It was observed from experiments that the indenter crushes the rock material directly beneath the contact surface as the impact progresses. Figure 11 shows the damaged zone in a impacted rock sample that broke into two pieces. As suggested for the static test, the crushed zone represents a "quasi–plastic" behaviour [23].

The indentation force–displacement response under impact loading is shown in Fig. 12 for three successive impacts of the sandstone. The impacts were at the same location on the surface of the sandstone. It is observed that the relationship between the force and the penetration is non–linear. The curves follow a similar trend to the response for the quasi-static test discussed earlier. It is noted that all frequencies applied resulted in similar type of damage of the sample surface. This is attributed to the fact that the frequencies applied were not too different: 3 Hz to 5 Hz. As a result of the speeds involved the unloading phase was not captured adequately by the LVDT.

The experimental data provides us with the opportunity to deduce a contact law which can be used in the dynamic model for percussive drilling. To achieve this, a similar relationship to that proposed by Andrews *et al.* [31] to represent the force–penetration of the impact of a sharp indenter on a rate sensitive elastic-plastic material at low impact speeds is put forward in the present study to represent the relationship between the indentation force and the displacement of a rigid indenter on a rock. This is based on earlier observations from the analysis of experiments that suggested that the static indentation of rock results in a "quasi–plastic" material response. The relationship between the indentation force F and the penetration δ is given as

$$F = C_1 \delta^n \left(1 + C_2 \delta'\right). \tag{14}$$

where δ' is the penetration velocity, and C_1, C_2 and exponent n are material constants which depend on the geometry of the indenter and material. These constants can be obtained by adapting equation (14) so that the linear least square method could be applied to fit the experimental data as similarly carried out for the static tests.

In order to accomplish this, equation (14) is re-written in the form

$$F = a x_n + b x_p. \tag{15}$$

where

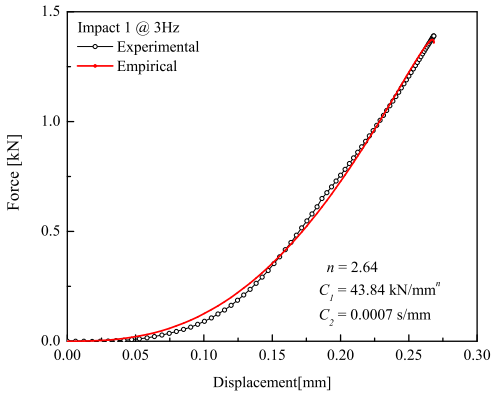

(a)

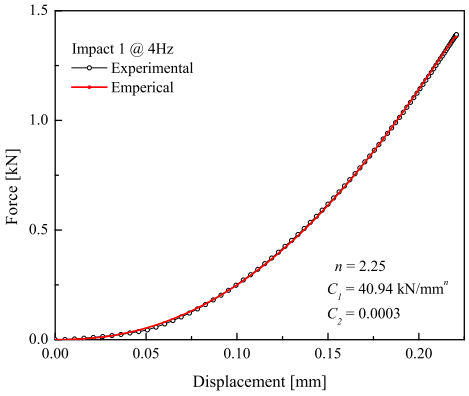

(b)

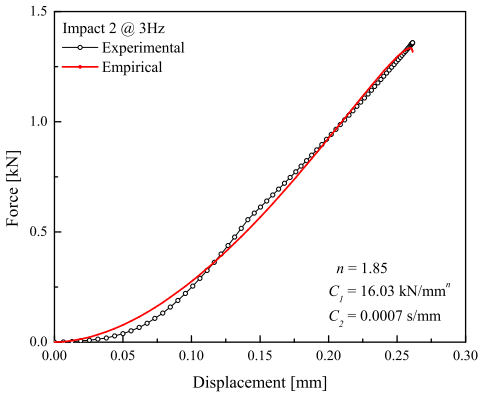

(c)

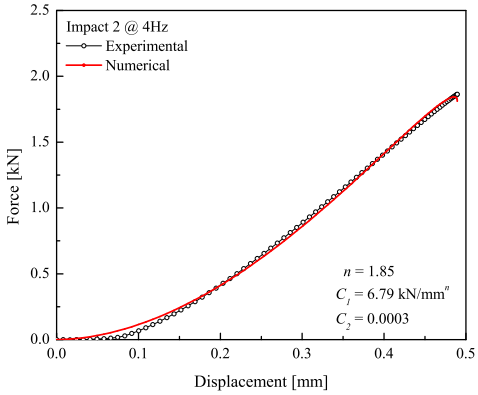

(d)

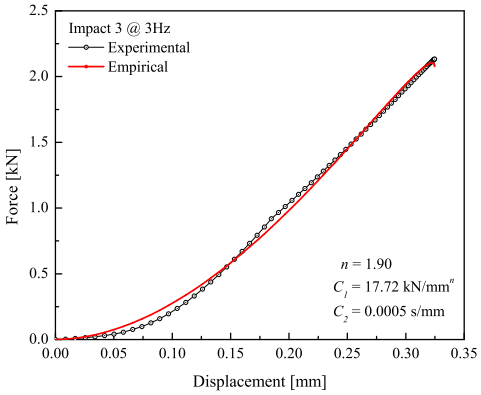

(e)

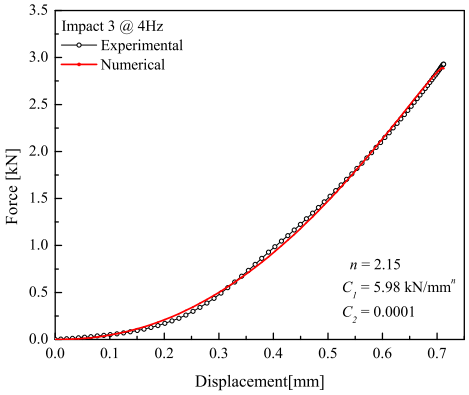

(f)

Figure 12. Force–displacement relationship for dynamic loading of sandstone at 3 Hz and 4 Hz, (a,b) first impact, (c,d) second impact and (e,f) third impact. All the impacts were at the same location.

$$x_n = \delta^n, \quad x_p = \delta^n \delta' \quad a = C_1, \quad \text{and } b = C_1 C_2.$$

Using the linear least square method [25], it can be shown that

$$a = \frac{1}{\sum x_n^2} \left[\sum x_n F - \frac{\sum x_n x_p \sum x_n F - \sum x_n^2 \sum x_p F}{\left(\sum x_n x_p\right)^2 - \left(\sum x_n^2\right)^2} \sum x_n x_p \right]. \tag{16}$$

$$b = \frac{\sum x_n x_p \sum x_n F - \sum x_n^2 \sum x_p F}{\left(\sum x_n x_p\right)^2 - \left(\sum x_n^2\right)^2} \tag{17}$$

Applying a similar approach as that discussed for the static tests, the value of n and the corresponding value of C_1 and C_2 that produce the best curve fit are those which give the minimum deviation between the prediction, eqn. (14), and the experimentally measured response. This implies that for assumed values of $n = n_i$ we estimate the corresponding value of a_i and b_i using eqns. (16) and (17) and the measured penetration δ, penetration velocity δ' and indentation force F. The square of the deviation, ζ_j, between the predicted force-displacement response using the estimated $n = n_i$, a_i and b_i in eqn. (14) and the measured response for the jth measured data point is given by

$$\zeta_j = \left(F_j - (a_i x_j + b_i x_j)\right)^2 \tag{18}$$

The maximum of value of the deviation for a given data set, D_i, is given by

$$D_i = \max\left[\zeta_j\right] \tag{19}$$

The chosen combination of n, C_1 and C_2 are those that minimise the deviation.

Figure 13 shows the variation in the value of the deviation D with n obtained for some of the experiments. For example, using the data for a test with impact velocity of 541 mm/s and operating frequency of 4 Hz, the maximum value of $\zeta = 0.005$ kN^2 at $n = 1.85$ which corresponds to the value of $C_1 = 6.79$ kN/mm$^{1.85}$ and $C_2 = 0.0003$ s/mm. This approach is applied to all the impacts to determine the values of n, C_1 and C_2.

Table 4 gives a summary of the values of C_1, C_2 and n obtained for the loading phase of a successive impacts. It is noted that the value of C_1 reduces after the first impact and soon attains a fairly constant value, while n has an average value of 2.10. It is observed that $C_2 \delta' \ll 1$. Thus, the second term in eqn. (14) can be neglected and we assume that similar force-displacement relationship exists for both the static and dynamic loading. It is also worth noting once again that expression for the force in terms of the penetration is thus approximately the same as that derived from

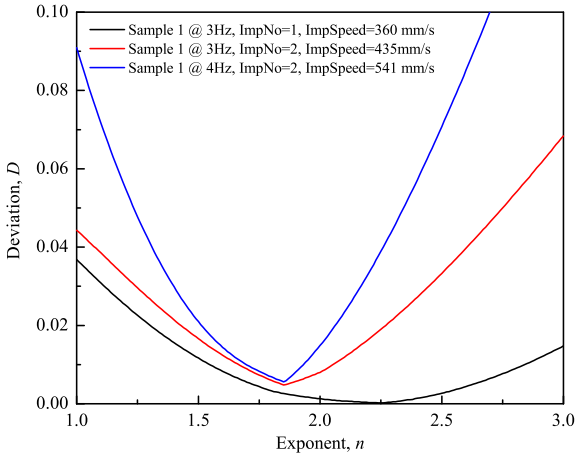

Figure 13. Graphical representation of the method of estimating of the best value of n for impacts at different impact velocities (D in kN^2).

Table 4
A summary of exponent n, and constants C_1 and C_2 values obtained from dynamic test during the loading phase.

Sample No.	Operating frequency [Hz]	Impact Number	Impact Velocity [mm/s]	n	C_1 [kN/mm^n]	C_2 [s/mm]
1	3	1	412	2.64	43.84	7×10^{-4}
1	3	2	435	1.85	16.03	7×10^{-4}
1	3	3	581	1.90	17.72	5×10^{-4}
1	4	1	361	2.25	40.84	3×10^{-4}
1	4	2	541	1.85	6.79	3×10^{-4}
1	4	3	686	2.15	5.85	1×10^{-4}
2	3	1	662	2.07	16.18	1×10^{-4}
2	3	2	829	2.50	15.40	1×10^{-4}
2	3	3	859	2.12	18.79	1×10^{-5}
2	4	1	1120	2.10	6.56	9×10^{-5}
2	4	2	1168	1.88	7.85	1×10^{-5}
2	4	3	1104	1.85	13.90	3×10^{-5}
2	5	1	1280	1.89	8.15	8×10^{-5}
2	5	2	1427	2.16	7.77	5×10^{-5}

theoretical studies. However, a look at Table 5 with the average value of these estimated parameters for the impact frequencies suggests the deviation from the mean values of C_1 are more significant than for K for the static loading

Table 5
A summary of the average values of exponent n, and constants C_1 and C_2 values obtained from dynamic test of sandstone during the loading phase.

Operating frequency [Hz]	n	C_1 [kN/mm^n]	C_2 [s/mm]
3	2.13 ± 0.44	25.86 ± 15.59	$(6 \pm 1) \times 10^{-4}$
4	2.08 ± 0.20	17.83 ± 19.94	$(2 \pm 1) \times 10^{-4}$
3	2.23 ± 0.23	16.79 ± 1.78	$(7 \pm 5) \times 10^{-5}$
4	1.94 ± 0.13	9.43 ± 3.92	$(4 \pm 4) \times 10^{-5}$
5	2.02 ± 0.19	7.96 ± 0.26	$(7 \pm 2) \times 10^{-5}$

(Table 3). This observation may be the consequence of rock heterogeneity and damage. As noted earlier, the value of parameter, C_1 remains relatively unchanged with increasing number of impacts.

It was pointed out earlier that the response could be predicted using static equation (3) for low velocity impacts. The impact velocities in Table 4 are significantly lesser than typical wave speeds. Hence dynamic test condition could be classified as nearly quasi-static. Furthermore, the results estimated for C_1 at 4 Hz and 5 Hz stays fairly constant after few impacts. Therefore, the values of C_1 and n estimated after five impacts could be used as material constants in any dynamic model developed for percussive drilling.

5. Conclusions

The experimental studies confirm that the force, F, versus displacement , δ, relationships for the indentation of rock from both static and dynamic loading follow a power–law relationship $F = K\delta^n$ and $F = C_1\delta^n$ respectively. The value of the exponent n obtained for both the static and dynamic tests have a value of about 2. This suggests that expression obtained using the elastic-plastic indentation theory reasonably agrees with the experimental observation. Hence, the force–displacement relationship based on existing theoretical derivation provides a reasonable approximation for the resisting indentation force of rock in numerical simulation aimed at capturing the dynamic response of the drilling module.

Furthermore, it is noted that the relationship proposed for the dynamic test does not really differ from that for the

static test. This confirms earlier studies that show that the rock fragmentation response does not differ significantly from quasi–static loading at impact velocities significantly lower than the wave speed in the rock. This observation is also a consequence of the fact that region of contact during the tests was several times smaller than the dimensions of the impacting bodies.

The current results are based on simplifying the response of the drillbit to that of a single indenter. Hence, the observation may differ for an actual drilling experiment. This is because the cutter or insert distribution on the drillbits may vary from one type to the other and their geometries are more complex than those used in these experiments. The best force–penetration response would be obtained from indentation tests using an actual drillbit. However, the results from the experiments provide the foundations for the parametric studies required for the design of a percussive drilling module.

References

[1] Mishnaevsky, L.L. (1998), "Rock fragmentation and optimization of drilling tools" in Aliabadi M.H. (ed.), *Fracture of Rocks*, Southampton, Computation Mechanics Publications.

[2] Pavlova, N.N. and Shrienerm L.A. (1964), *Rock Fracture in Dynamic Loading.* Moscow, Nedra.

[3] Artsimovich, G.V., Poladk, E.N., Sveshnikov, I.A. (1978), *Investigation and development of Rock Breaking Tools for Drilling*, Nauka, Novossibirisk.

[4] Blokin, V.S. (1982), *Improvement of Drilling Tool Efficiency*, Kiev, Teknika.

[5] Nikiforovsky, V.S., Shemyakin T.I. (1952), *Impact Fracture of Solids*, Nauka, Novossibirisk.

[6] Eigheles, R.M. (1971), *Rock Fracture in Drilling*, Moscow, Nedra.

[7] Franca, L.F.P., (2011), " A bit–rock interaction model for rotary percussive drilling, " *Int. J. Rock Mech. Min. Sci.*, 48, pp. 827-835.

[8] Wiercigroch, M., Wojewoda, J., Krivtsov, AM. (2005) "Dynamics of ultrasonic percussive drilling of hard rocks". Journal of Sound and Vibration, vol 280, no. 3-5, pp. 739-757.

[9] Pavlovskaia, E.E., Wiercigroch, M., Woo, K–C. and Rodger, A.A. (2003), "Modelling of ground moling dynamics by an impact oscillator with a frictional slider," *Meccanica*, 38, pp. 85-97.

[10] Franca, L.F.P. and Weber, H.I. (2004), " Experimental and numerical study of resonanance hammer drilling model with drift," *Chaos Solitons & Fractals*, 21, pp. 789–801.

[11] Mishnaevsky, L.L. (1993), "A brief review of soviet theoretical approaches to dynamic rock failure," *Int. J. Rock Mech Min Sci.*, 30 (5), pp. 663-668.

[12] Mishnaevsky, L.L. (1995), "Physical mechanism of hard rock fragmentation under mechanical loading: a review," *Int J. Rock Mech Min Sci.* 32 (8), pp. 763-765.

[13] Love, A.E.H.(1906), *A treatise on the mathematical theory of elasticity*, Cambridge, Cambridge Univ. Press.

[14] Villaggio, P. (1996), " The rebound of an elastic sphere against a rigid wall," *Journal of Applied Mechanics*, 63, pp. 259–263.

[15] Johnson, K.L. (1970), "The correlation of indentation experiments," *J. Mech. Phys. Solids*, 7, pp. 115-126.

[16] Tabor, D., 1951, *The Hardness of Metals*, Oxford Univ. Press, Oxford.

[17] Mulhearn, T.O., (1951), " Deformation of Metals by Vickers-Type Pyramidal Indenters." *J. Mech. Phys. Solids*, 18, pp. 85–96.

[18] Stronge, W.J., (2000),*Impact Mechanics*, Cambridge Univ. Press, Cambridge.

[19] Johnson, K.L. , (1985), *Contact Mechanics*, Cambridge Univ. Press, Cambridge.

[20] Mesarovicy, S.D. and Fleck, N.A., (1999), "Spherical Indentation of Elastic-Plastic Solids", *Proc. R. Soc. Lond.*, A 455, pp. 2707–2728.

[21] Pang, S.S., Goldsmith, W.and Hood, M., (1989), "A Force–Indentation Model for Brittle Rocks", *Rock Mech. Rock Engrg.*, 22, pp. 127–148.

[22] Szwedzicki, T. (1998), "Indentation hardness testing of rocks," *Int. J. Rock Mech. Min Sci.*, 6, pp. 825-829.

[23] Lawn, B.R. (1998), " Indentation of Ceramics with Spheres: A century after Hertz," *J. Amer. Ceramic Soc*, 81 (8), pp. 1977–1994.

[24] Stroud, K. (1995), *Engineering Mathematics*, 4th Edition, London, Macmillan

[25] Kick, F. (1885), *Das Gesetz der proportionalen Widerstȃnde und seine Anwebdungen*, Leipzig, Felix-Verlag

[26] Meyer, E. (1908), *Untersuchungen uber Harteprufung und Harte. Z. Ver. Deutche Ing*, 52, 645–654.

[27] Attaf, M.T. (2004), "Connection between the loading curve models in elastoplastic indentation," *Materials Letters*, 58 , pp. 3491–3498.

[28] Ajibose, O.K.,Wiercigrich. M., Akisanya A.R., "Experimental determination of the plastic properties of sandstone" (To be submitted)

[29] Doebelin, E. O. (1983), *Measurement Systems Application and Design*, 3rd Edition, New York, McGraw Hill.

[30] Sakai, M. (2003), "Elastic recovery in the unloading of pyramidal microindentation," *J. Material Res.*, 18, pp. 1631-1640.

[31] Andrews, E.W., Giannakopoulos, A.E. , Plisson, E. and Suresh, S. (2004), " Analysis of the impact of a sharp indenter," *Int. J. Solids Struct.*, 39, pp. 281-295.